EUROPEAN ORGANIZATION FOR NUCLEAR RESEARCH
CERN — BEAMS DEPARTMENT

BE-Note-2009-022

Comparison of LINAC-4 Designs

J. Stovall, K. Crandall, E. Sargsyan, J-B Lallement

Abstract

We have studied the expected performance of two drift tube linac (DTL) designs proposed for LINAC-4. The two designs use the same cell geometries but are characterized by different phase (φ_s) and accelerating field (E_0) distributions. In addition we have investigated the expected performance of 3 different quadrupole focusing schemes in each design. The expected performance of these 6 variants is compared with respect to their stability and risk of beam loss with alignment errors.

Geneva, Switzerland
June, 2009

1. Introduction

We are studying the expected performance of two drift tube linac (DTL) designs proposed for LINAC-4. The two designs use the same cell geometries but are characterized by different phase (φ_s) and accelerating field (E_0) distributions in the first tank. In addition we have investigated the expected performance of 3 different quadrupole focusing schemes in each design. In this study we refer to the first DTL design as the "Baseline" design. A more recent variant of this design, we refer to as the "Reference" design.

2. Design and analysis tools

Detailed designs have been generated for both the Baseline and Reference DTLs using the code GENDTL (1). In addition we have used a spread sheet program that has become a useful tool for exploring the DTL parameter space and analyzing the resulting first-order performance of design examples. We refer to this program as DTLTOOL (2).

DTLTOOL requires a description of the geometry-related parameters T, Z & E_{peak} in the form of polynomial fits in β. These values are normally derived from SUPERFISH (3), however, in this case they have been supplied directly from the GENDTL designs. Figure 1 shows the transit time, T, plotted as a function of β in the Baseline design.

The value for shunt impedance, ZT^2, calculated by SUPERFISH includes the effects of drift tube stems and end walls. To account for the effects of the post couplers, tuners, power coupler, surface effects, operating temperature, etc, ZT^2 has been reduced by 20%, in effect increasing the power requirements by 25%. Figure 2 shows the shunt impedance, ZT^2 which has been reduced 20% from the SUPERFISH value, plotted as a function of β in the Baseline design.

Since the Baseline and Reference designs use essentially the same cell geometries, but have different number of cells per tank, these curves look very similar for both linac designs. In these plots the values corresponding to β_{in}, generated by GENDTL, are plotted in color. The "outliers" correspond to cells that have been modified to facilitate longitudinal matching between tanks. We have fit 4th order polynomials to this data, excluding the outliers, which are used in DTLTOOL. The open circles are the values corresponding to β_{ave} in the cells generated by DTLTOOL.

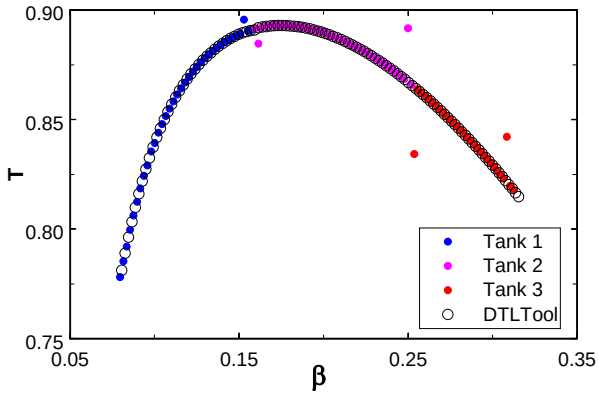

Figure 1. Baseline Transit Time Factor

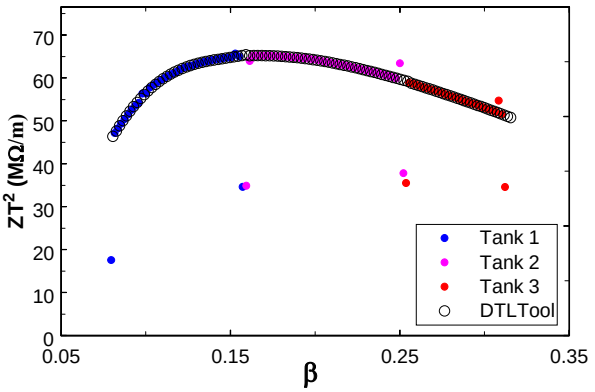

Figure 2. Baseline Shunt Impedance 80% of SUPERFISH Value

3. DTL Designs.

Both DTL designs are characterized by a phase ramp in tank 1. In the Baseline design the synchronous phase is ramped from -30° to -20° over the first 21 cells as shown in figure 3. To increase the longitudinal acceptance in the Reference design and make it less sensitive to rf phase and amplitude errors, the synchronous phase is ramped form -40° to -26.8° over the entire length of the tank, 45 cells, as shown in figure 4. We can see in these two plots how φ_s, at the ends of adjacent tanks, has been reduced to compensate for the missing gaps between tanks. The colored points are those generated by GENDTL while

the open circles are those generated by DTLTOOL in which case, the phase matching considerations have been neglected.

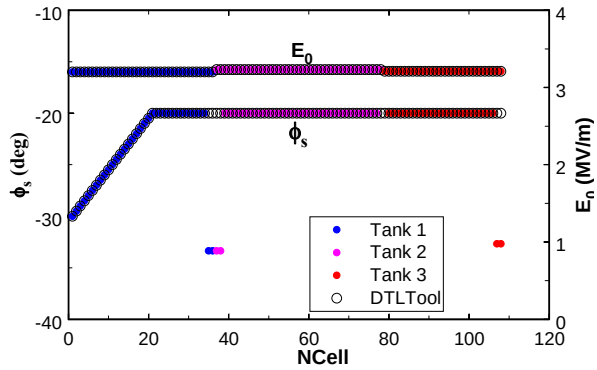

Figure 3. Baseline φ_s & E_0 Laws

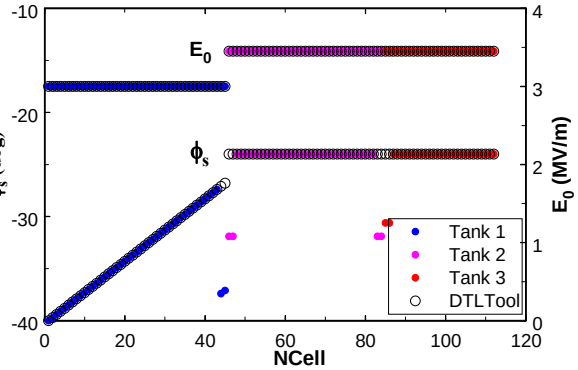

Figure 4. Reference φ_s & E_0 Laws

DTLTOOL generates DTL cells by calculating the energy gain cell by cell based on the equation $\Delta W = qE_0TL\cos(\varphi_s)$, where φ_s and E_0 are linear functions of the cell number and are specified by the user. In this case they were generated by GENDTL. T is evaluated from a polynomial for the average cell velocity, β_{ave}. L, the cell length, is defined to be equal to $\beta_{ave}\lambda$. The code makes an initial guess for the cell length and then iterates, with T and L being reevaluated from β_{ave} on each iteration, until it converges.

Tables 1 and 2 summarize the properties of the Baseline and Reference designs as generated by DTLTOOL. Tables 3 and 4 summarize the Baseline and Reference designs as generated by GENDTL. The power includes both the rf power required to excite the cavities plus the power required to accelerate the beam. For the beam power we have assumed a peak current of 64 mA reduced by a chopping factor of 5/8 for an average macro-pulse current of 40 mA.

Table 1. DTLTOOL Baseline Design Summary

Tank	No of Cells	Length m	W_{final} MeV	Power MW
1	36	3.64	12.30	0.832
2	42	7.46	32.30	1.766
3	30	7.32	50.83	1.713
total	108	18.42	50.83	4.31

Table 2. DTLTOOL Reference Design Summary

Tank	No of Cells	Length m	W_{final} MeV	Power MW
1	45	4.63	13.10	0.915
2	39	7.03	32.65	1.767
3	28	6.84	50.78	1.807
total	112	18.51	50.78	4.49

Table 3. GENDTL Baseline Design Summary

Tank	No of Cells	Length m	W_{final} MeV	Power MW
1	36	3.63	12.18	.856
2	42	7.41	31.80	1.786
3	30	7.27	50.00	1.740
total	108	18.31	50.00	4.382

Table 4. GENDTL Reference Design Summary

Tank	No of Cells	Length m	W_{final} MeV	Power MW
1	45	4.62	13.00	.937
2	39	7.00	32.34	1.844
3	28	6.81	50.31	1.797
total	112	18.43	50.31	4.578

We see that there are slight differences in the designs resulting from these two approaches. The DTLTOOL design is based on a simple 1st order analytical approach while GENDTL uses much more mathematically rigorous algorithms. Even so, there is <0.5% difference in overall linac length between the designs generated by the two codes. There is also <2% difference in the predicted power requirements "at the RF window." This is due to the fact that DTLTOOL does not generate the special cells to accommodate inter-tank matching which reduces their efficiency thus requiring more power. Additional power will be required for waveguide and circulator losses and control margin.

4. Beam Dynamics Properties in the Baseline Design.

We first look at the beam dynamics properties of the Baseline design for which we have studied two quadrupole laws. In the first case we use an FDFD (+-+-) quadrupole lattice in all 3 tanks while in the second case we have used an FFDD (++--)lattice in the first tank to more closely approximate the period of the MEBT and accommodate a smoother match. The quadrupoles in tank one are half the length of those in tanks 2 and 3 in both designs. Figures 5 and 6 show the quadrupole gradients in the Baseline design for the two lattice options. The colored points are the gradients generated by TRACEWIN (1) while the open circles are the values derived from a quadratic fit in β to these values used by DTLTOOL. Note that quads in the ends of adjacent tanks have been used to match the beam between tanks. These "outliers" have not been included in the fit nor in the DTLTOOL design.

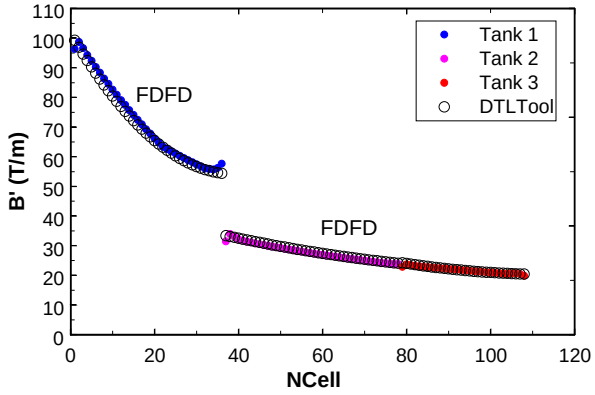

Figure 5. Baseline design, FDFD Lattice Gradients

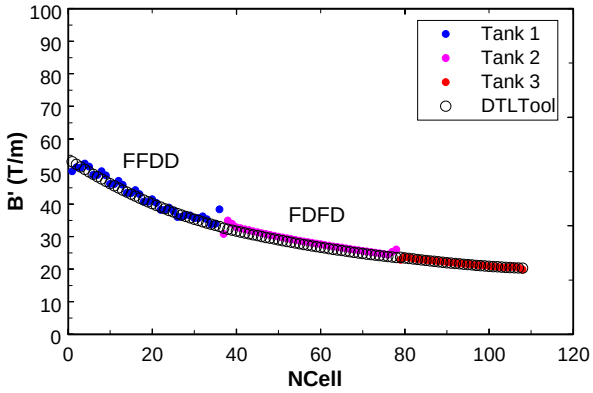

Figure 6. Baseline Design FFDD Lattice Gradients

The discontinuity in the FDFD case reflects the fact that the quadrupole lengths are doubled in tank 2. The gradients in the FFDD case appear to lie on a smooth curve because both the magnet length and the periodicity change by a factor of 2 in the second tank. We characterize the focal properties of the lattice in terms of phase advance without and with space charge. To evaluate these properties we have applied the envelope equations from TRACE3-D **(4)** to construct a period representative of each DTL cell. By finding the matched beam for that representative period we can derive the zero-current phase advance, σ_0, corresponding to each cell. From that, the code estimates the corresponding phase advance including the effect of beam current σ. Figures 7 and 8 show the zero-current phase advance per lattice period (°/period) for the two lattices. The magenta curve represents the longitudinal motion, σ_{0l}, while the blue curve represents the transverse motion, σ_{0t}. Note that the lattice periods in the first tank are 2 and 4 cells long in the FDFD and FFDD designs respectively.

From these plots we can see that in no case do the curves cross 90° nor is one equal to twice or half the value of the other. We do not, therefore, expect to encounter any parametric resonances in either design. Figures 9 and 10 show the tune depression for a beam having a peak current of 64 mA approaching 50%-60% in the transverse and longitudinal planes respectively which is a high but reasonable value.

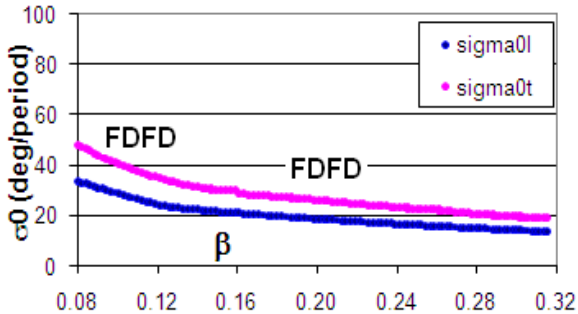

Figure 7. Zero-Current Phase Advance per Period for Baseline FDFD Design

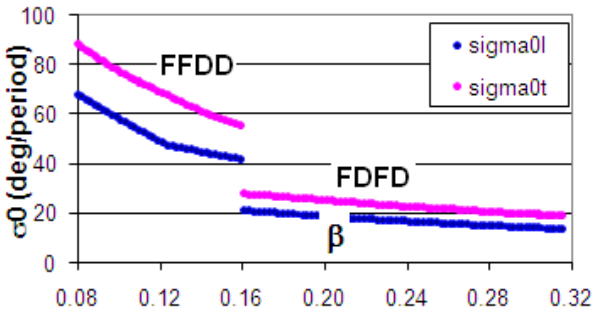

Figure 8. Zero-Current Phase Advance per Period for Baseline FFDD Design

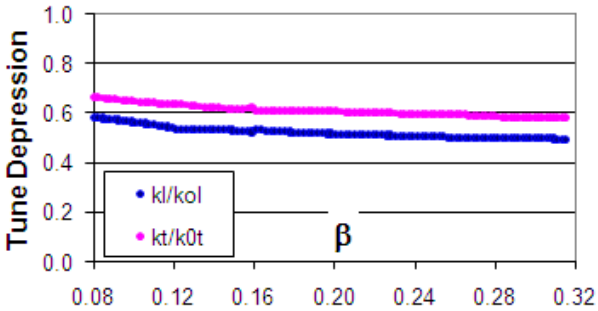

Figure 9. Baseline FDFD Tune Depression at 64 mA

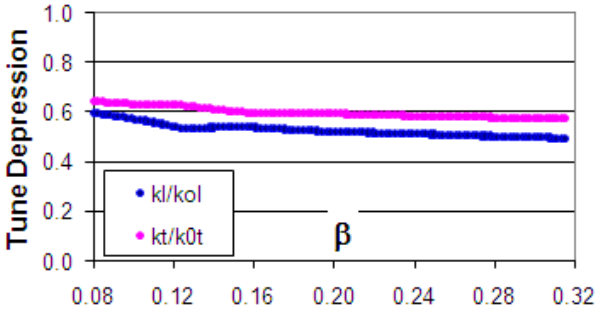

Figure 10. Baseline FFDD Tune Depression at 64 mA

The "strength" of a lattice is characterized by its "real-estate" phase advance, k (°/m) which is plotted in Figures 11 and 12 at full beam current. Even though the quadrupole gradients in the FFDD design are half the value of those in the FDFD design, these curves show that the two designs provide essentially the same beam confinement. Because both curves in both cases are smooth and continuous we can expect both designs to be "current independent."

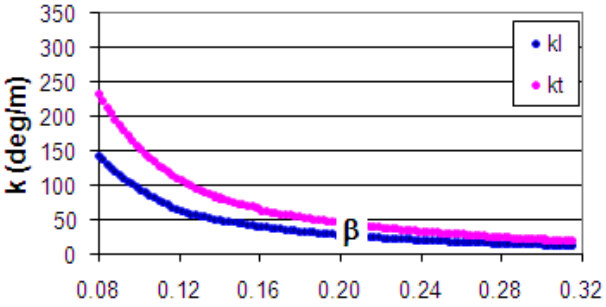

Figure 11. Baseline FDFD Real-Estate Phase Advance

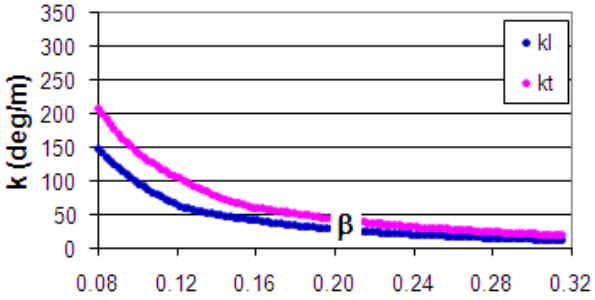

Figure 12. Baseline FFDD Real-Estate Phase Advance

Figures 13 and 14 shows the equipartitioning ratio, $(\varepsilon_{0l}\,\sigma_l)/(\varepsilon_{0t}\,\sigma_t)$, at full current (64 mA) to be close to unity throughout the linac implying that, with a well-matched initial beam, we should expect minimal emittance growth due to energy exchange between planes in both designs.

Although linacs are short relative to circular machines, in which beams pass through the same lattice millions of times, we try to design them so that the coupled transverse and longitudinal motion does not lie close to known resonance bands. Hofmann (5) has shown that certain instabilities can be excited in current-dominated beams in only a few betatron periods. Figures 15 and 16 show the Hofmann Diagram in which the resonance bands of concern are shown schematically in blue. We see in these plots that the longitudinal and transverse focusing has been balanced so that the resulting coupled motion lies just between the 3rd and 4th bands. By slightly reducing the quadrupole gradients, moving the design point in the Hofffman diagram to the right, we can bring the equipartitioning ratio close to unity. If, however, the longitudinal emittance is larger than expected, as it seems to be in the US-SNS linac (6), having a slightly depressed equipartitionong ratio is the correct design.

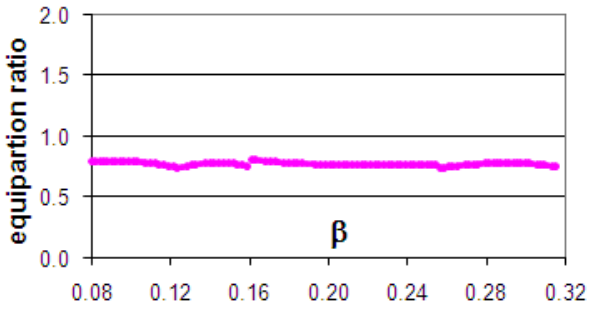

Figure 13. Baseline FDFD Equipartitioning ratio

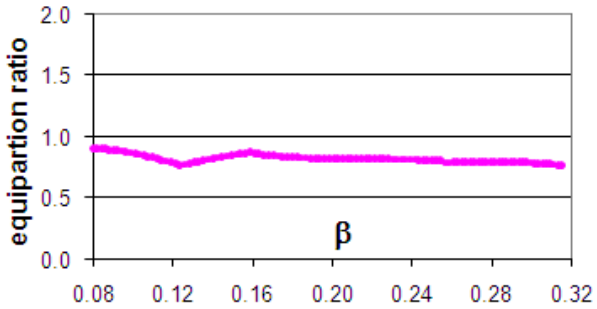

Figure 14. Baseline FFDD Equipartitioning Ratio

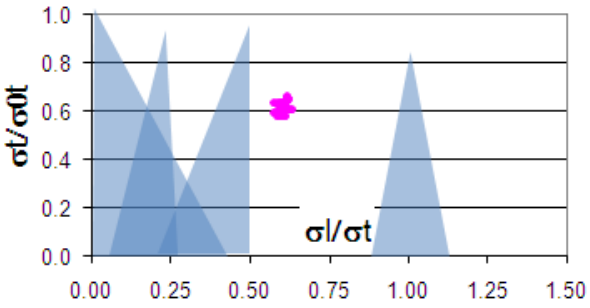

Figure 15. Baseline FDFD Hofmann Diagram

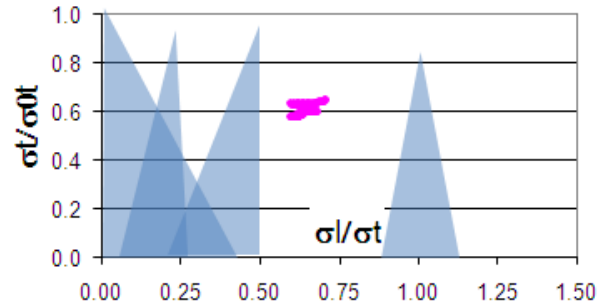

Figure 16. Baseline FFDD Hofmann Diagram

Figures 17 and 18 show that the nominal beam size, in both transverse and longitudinal dimensions, should be about the same in both designs.

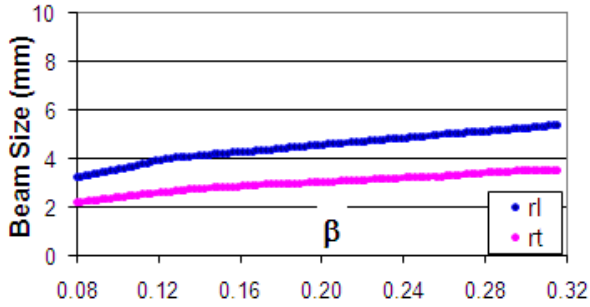

Figure 17. Baseline FDFD Equivalent Uniform Beam Size

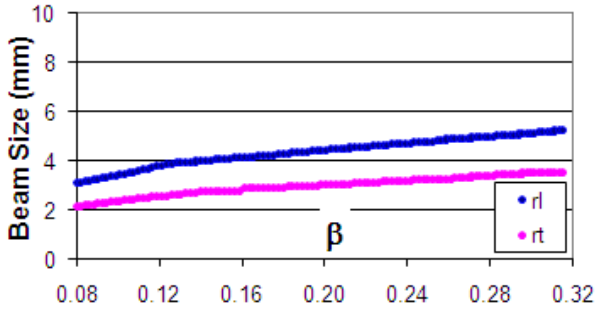

Figure 18. Baseline FFDD Equivalent Uniform Beam Size

5. Alignment Errors in the Baseline Design.

Errors in the alignment of the individual quadrupole magnets will cause the beam to be displaced from, and oscillate about the linac axis. Errors in focusing strengths cause the beam to become mismatched to the system and cause the beam envelope to oscillate about its ideal size. Both types of errors can lead to beam loss and emittance growth if the errors are too large.

If the quadrupoles are perfectly aligned, a beam injected on axis will remain on axis. If the beam is injected off axis, the beam's centroid will oscillate with an amplitude proportional to its initial coordinates (displacement and angle). If, in addition, the lenses are randomly displaced from the axis, the oscillation amplitude will be modified at each displaced lens. Whether the amplitude is increased or decreased at any lens will depend on the coordinates of the beam centroid and on the direction of the lens displacement. If the oscillation amplitude is already large when the beam arrives at a displaced lens, the displacement has an almost equal probability of increasing or decreasing the oscillation amplitude, although there is a higher probability that the amplitude will be further increased. In this section we consider the consequences of misaligned quadrupoles without steering corrections.

In this study we calculate an "expected value" for the oscillation amplitude of the beam centroid at each cell in the linac for a specified alignment tolerance. The expected value, in this case, means that there is a 65% probability that the oscillation amplitude will be less than this value, and a 35% probability that it will be greater than this value. There is a 90% probability that the oscillation amplitude will be less than 1.5 times the expected value, and a 95% probability that it will be less than 1.7 times the expected value. (These values were determined from computer simulations.)

For a sequence of N quadrupoles having a random displacements from a smooth curve, the expected value for the square of the oscillation amplitude at the n^{th} lens is:

$$\left\langle A^2 \right\rangle = \frac{\beta_N}{\eta_N}\frac{\eta_0}{\beta_0}\left\langle A_0^2 \right\rangle + \left\langle (\delta x)^2 \right\rangle \frac{\beta_N}{\eta_N}\sum_{n=1}^{N}\frac{\eta_n \beta_n}{f_n^2},$$

where $\langle\ \rangle$ denotes expected values. A_0 is the initial oscillation amplitude, η_n is the product of the relativistic parameters β and γ, β_n is the matched ellipse parameter (for zero current) at the lattice period starting with the n^{th} quadrupole having a focal length f_n. β_N and η_N are the values corresponding to the final period in the multi-period lattice being evaluated. $\left\langle (\delta x)^2 \right\rangle$ is the expected value of the squared displacement of the quads.

There are three sources of manufacturing and assembly errors that add in quadrature that will affect the alignment of the magnetic axis of the PMQs in the linac. We estimate that, with realistic tolerances, we can expect the magnet axis to be collinear within a truncated Gaussian distribution having σ=0.1 mm and extending to 3σ or ±0.3 mm. DTLTOOL calculates the "expected" centroid excursion that the beam will experience assuming an initial transverse beam displacement and a uniform distribution of randomly misaligned quadrupoles.

The expected centroid excursion is plotted in figures 19 and 20. In these two plots we have applied an alignment tolerance in the form of an "equivalent" uniform distribution of errors between ±0.173 mm (√0.03), which is equivalent to a Gaussian distribution of σ=0.1 mm, and an initial transverse beam displacement of 0.3 mm. The effect of this small centroid offset is negligible in all the cases studied. This method does not include the effect of an angular error in the initial centroid trajectory.

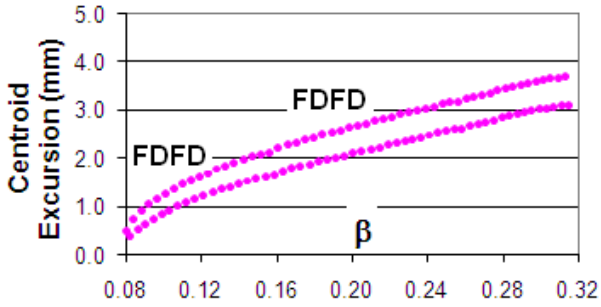

Figure 19. Baseline FDFD Expected Centroid Excursion with Errors

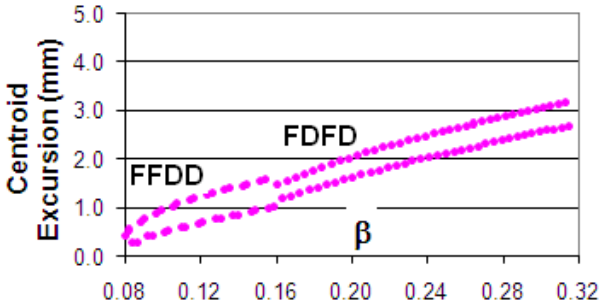

Figure 20. Baseline FFDD Expected Centroid Excursion with Errors

The fact that there are two curves in these figures is an artefact of the method, reflecting the fact that the matched β_n is different in the lattice periods beginning with either a focusing or a defocusing lens. It appears, from these plots, that the FFDD lattice in tank one is preferable because it is slightly less sensitive to misaligned lenses, resulting in a smaller centroid excursion throughout. The beam in the FFDD lattice has a larger "flutter factor" (waist to bust) in tank 1 but the two beams at their bust remain about the same size throughout the rest of the linac as we see in figures 21 and 22.

In these figures we have plotted the beam sizes corresponding to a uniform particle distribution (uniform in any 3-D volume) having an emittance of 5 rms. In general, the beam extent in any direction is equal to $\sqrt{\beta\varepsilon}$, so for this uniform beam, its rms size is proportional to $\sqrt{5\varepsilon_{rms}}$. We have specified a beam extent in the transverse direction of 3σ for the filling factor (F_{max}) calculation which is equal to √9/5 of the equivalent

uniform size. In other words we are using a uniform beam having an emittance of 5rms to simulate a Gaussian beam having an emittance of 9 rms to get its transverse size at 3σ. The expected filling factors are plotted for both designs in figures 23 and 24. We define an F_{max} of 1.0 to mean that the edge of a displaced beam would just touch the drift tube bore. If the edge of the beam extends beyond the bore we would expect to lose beam inside a 3σ perimeter. In these designs the maximum expected filling factor, occurring at the linac exit is 89% and 84% for the for the FDFD and FFDD designs respectively.

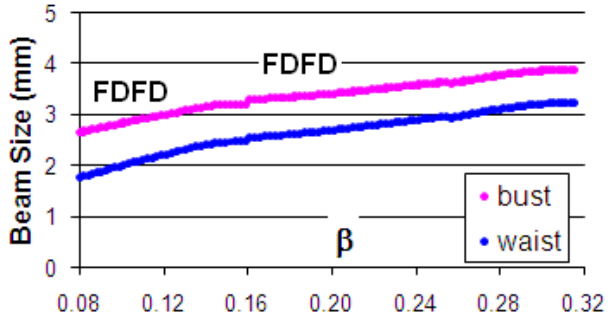

Figure 21. Baseline FDFD Equivalent Uniform Beam Size

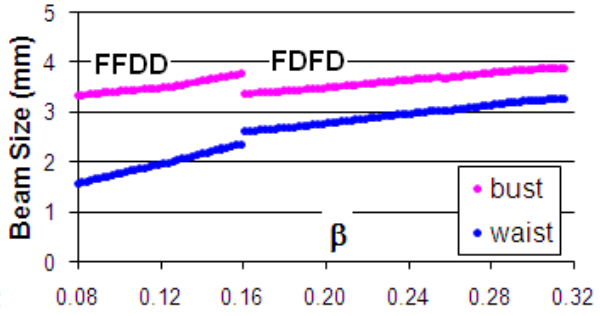

Figure 22. Baseline FFDD Equivalent Uniform Beam Size

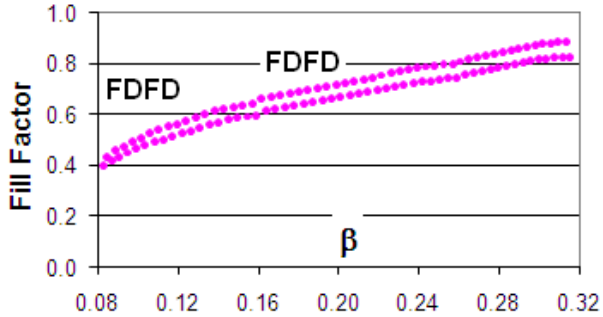

Figure 23. Baseline FDFD Expected Filling Factor for a 3σ Gaussian Beam

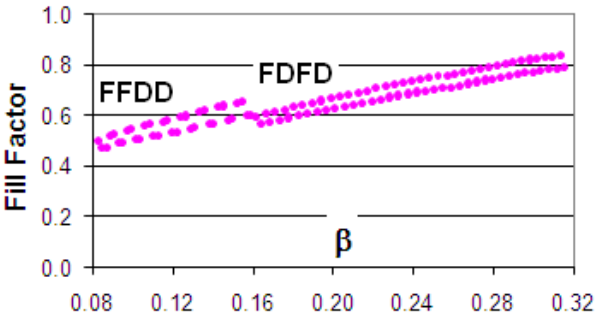

Figure 24 Baseline FFDD Expected Filling Factor for a 3σ Gaussian Beam

Since we can't predict exactly how the misalignments will be distributed it is more helpful to look at the problem of alignment statistically. We have used the code LTRACE (7) that follows a 6-D beam ellipsoid through the linac in which we have imposed quadrupole displacements randomly selected from within a specified tolerance. We typically run LTRACE with 1000 different sets of random errors, recording the maximum centroid excursion and filling factor for each run. By sorting the results we can produce the probability plots of these values shown in figures 25 and 26. We have assumed an rms normalized emittance of 0.31πmm-mR and transported a matched beam through the Baseline FFDD design. We have applied random displacement errors from both Gaussian, truncated at 3σ, and uniform distributions, both having the same standard deviation, σ=0.1mm. These plots do not include the effect of an initial beam displacement.

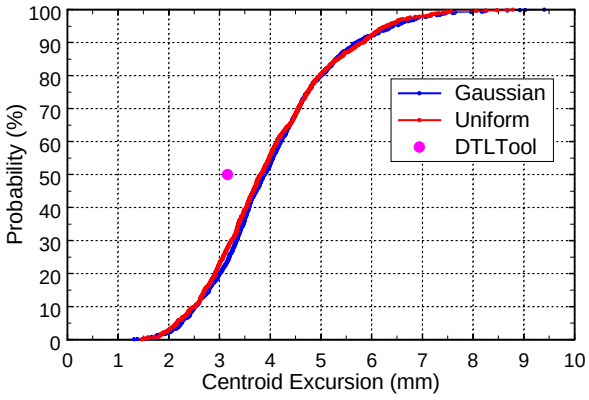

Figure 25. Baseline FFDD Centroid Excursion

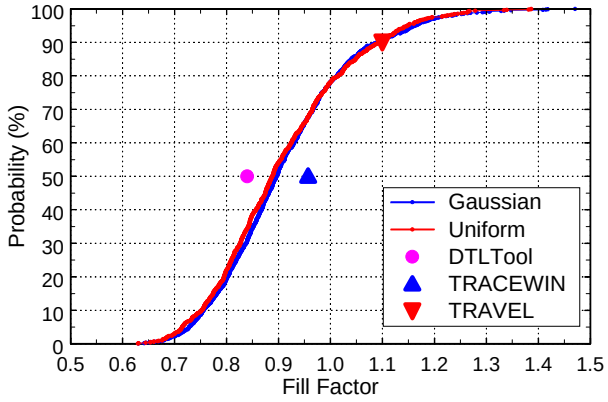

Figure 26. Baseline FFDD Filling Factor Probability

These figures show the probability that a set of errors in manufacturing and assembly will result in a matched beam having a maximum centroid excursion or filling factor less than the abscissa value. First we can see that any difference between uniform and truncated Gaussian error sets, having the same standard deviation, is statistically indistinguishable.

Figure 25 predicts that, at the 50th percentile, we can expect the beam centroid to have a maximum excursion of ~3.8 mm somewhere in the linac, somewhat more pessimistic than that predicted by DTLTOOL at the linac exit as we see in figure 20. With 90% probability, the centroid would stay within ~5.7 mm.

In figure 26 we show the filling factor corresponding to a beam having an emittance extending to 3 rms. It shows that with 20% probability the beam would fill no more than 80% of the drift tube bore at any one point in the linac. The "expected" value, or with 50% probability, the beam would fill no more than ~89% of the bore. This is in reasonable agreement with DTLTOOL that predicts a slightly more optimistic value factor of 84% as we see in figure 24. According to this analysis there is about a 20% chance that we could be so unfortunate to have misalignments that resulted in the 3σ beam touching or exceeding the 1 cm radius bore.

The beam will not necessarily have the largest filling factor in the last cell as DTLTOOL assumes. Figure 27 shows where the largest filling factors occur in the 1000 cases corresponding to the probability chart above. Note that the maximum filling factor occasionally occurs at the ends of tanks 1 and 2 where the matching quads break the otherwise periodic lattice.

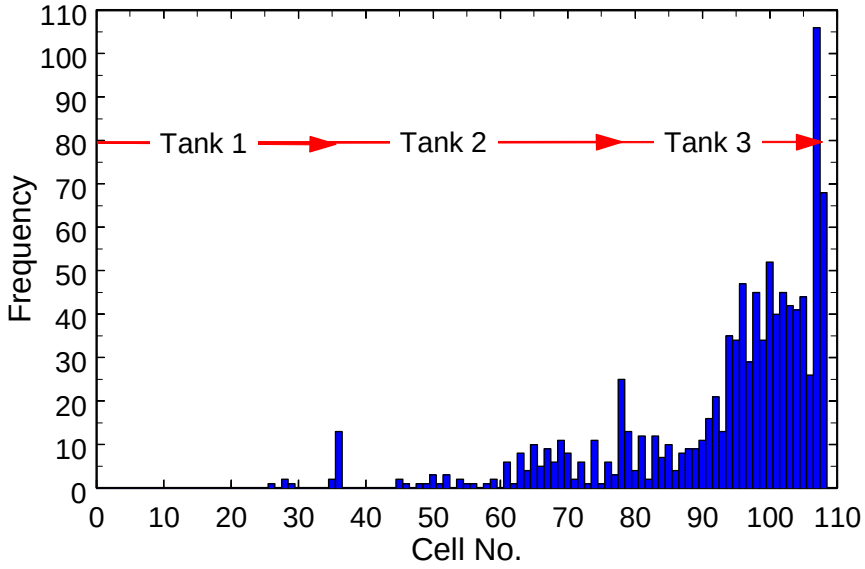

Figure 27. Baseline FFDD Location of Maximum Filling Factor

In an attempt to calibrate this analysis we have looked at the output distributions from TRACEWIN simulations using a 44k particle beam distribution originating with a 4-D uniform particle distribution at the ion source and transformed through the LEBT, RFQ and chopper line. Figure 28 shows the vertical beam profile in the final (defocusing) quad in the FFDD Baseline design. The exit beam appears to be quite Gaussian with a size at 3σ=6.42 mm 23% larger than the final beam size of 5.21 mm calculated by DTLTOOL for a matched ellipse.

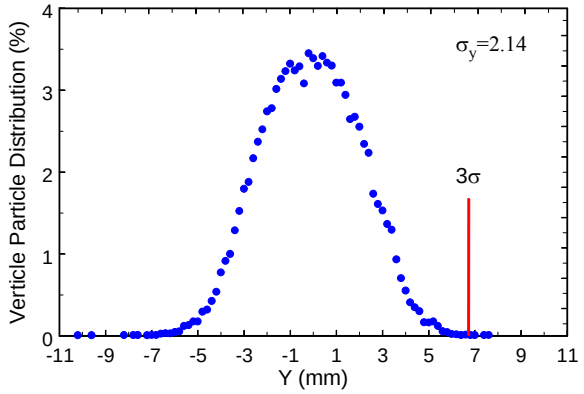

Figure 28. Vertical Beam Profile in Final Quad of the Baseline FFDD Calculated by TRACEWIN

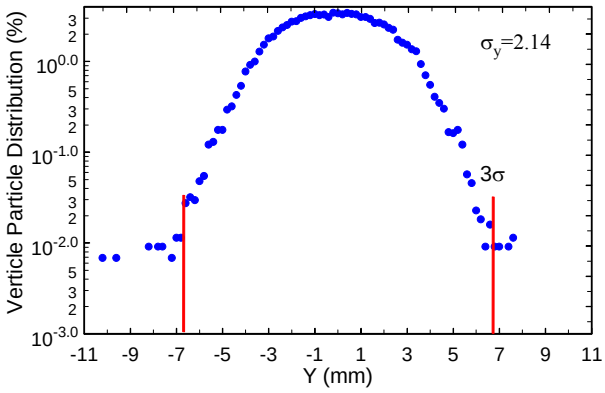

Figure 29. Log Plot of Vertical Profile in the final Quad of the Baseline FFDD

If we assume the expected value for the beam centroid excursion calculated by DTLTOOL and the 3σ beam size from TRACEWIN, we would expect a filling factor of 96% in the last drift tube. This points is plotted in figure 26 at the 50th percentile. Using a "matched generated beam" containing 44k particles at the linac entrance we have simulated the transmission through the linac with 1000 sets of misalignments (σ=±0.1mm within a truncated 3σ Gaussian) using the code TRAVEL (8). In addition, the initial beam centroid in the TRAVEL simulations was randomly displaced in both position and angle (σ=±0.3mm and ±0.3 mR within a truncated 3σ Gaussian). We find that with 90% probability, the filling factor reaches 1.1, in excellent agreement with LTRACE. From the TRAVEL simulations we can say qualitatively that the consequence of an angular error in the initial beam centroid dominates that of a lateral displacement within these tolerances.

Figure 29 shows the same profile data plotted on a log scale to magnify the halo. We see that we can expect ~0.17% of the beam to extend radially to almost 5σ. This halo represents ~70μA pulsed. The outermost particles in this 44k simulation with no errors lie 1 mm beyond the clear bore of the final drift tube. We have not studied the SPL beam which, while having a significantly higher duty factor, will be much less space-charge dominated and probably a smaller halo.

Based on these analyses and our present understanding of beam dynamics in linacs, we can conclude that both of these designs are generally conservative with respect to the selection of restoring forces, stable motion and the avoidance of potential resonances. We can also conclude that the two Baseline linac designs, differing only in the lattice in tank one, should have very similar performance with the FFDD case being slightly "safer" with respect to potential beam loss.

6. Beam Dynamics Properties in the Reference Design.

Next we looked at the beam dynamics of the Reference design for which we have studied the same two quadrupole laws, FDFD and FFDD in tank 1. The equipartitioning ratio is a very good figure of merit for DTL designs because it integrates over the transverse and longitudinal motion. Figures 30 and 31 show this ratio at full current (64 mA) to be slightly depressed from unity throughout the linac implying that, if the longitudinal emittance is in fact larger than expected, with a well-matched initial beam, we should still expect minimal emittance growth due to energy exchange between planes in both Reference designs. Figures 32 and 33 show the Hofmann Diagrams for the two designs with the coupled motion safely lying between the resonance bands.

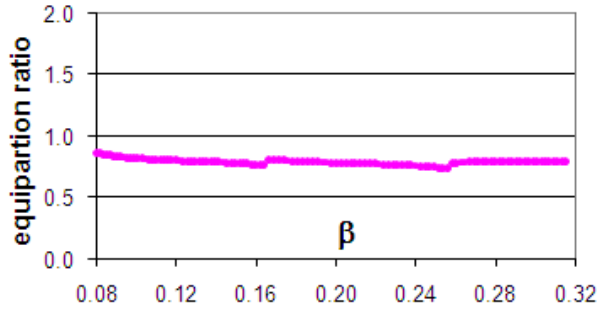

Figure 30. Reference FDFD Equipartioning Ratio

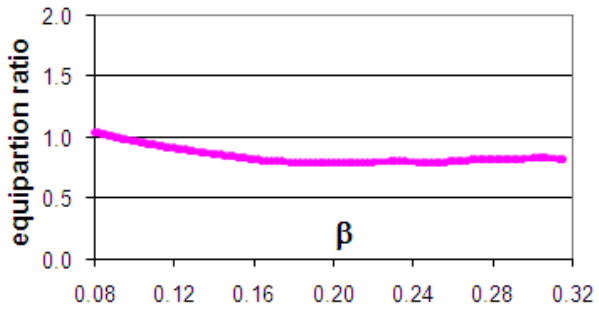

Figure 31. Reference FFDD Equipartitionong Ratio

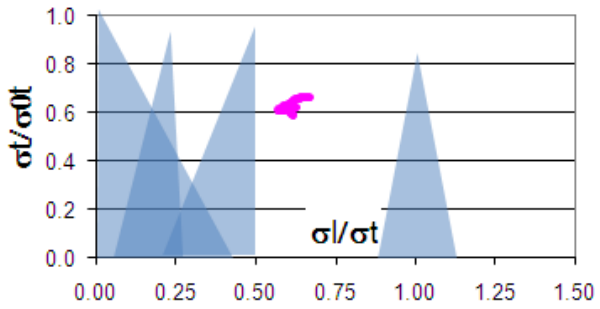

Figure 32. Reference FDFD Hofmann Diagram

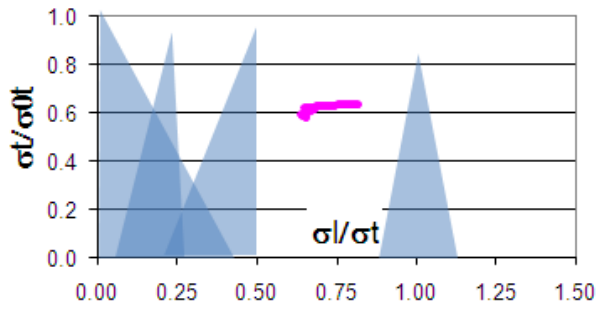

Figure 33.Reference FFDD Hofmann Diagram

In the FFDD design we were unable to maintain a constant ratio between the longitudinal and transverse restoring forces, σ_{0l}/σ_{0t}, in the beginning of tank 1 without crossing σ_{0t}=90°, and risking the excitation of a known instability. We see the result on figure 31 by the fact that the equipartitioning ratio has a negative slope in tank 1. In figure 33 we can see that the locus of the design point moves from right to left on the Hofmann Diagram in tank 1.

7. Alignment Errors in the Reference Design.

The expected centroid excursion for both Reference designs, based on a uniform set of randomly misaligned quadrupoles with σ=0.1 mm, is shown in figures 34 and 35. Here we see that the centroid excursion is dominated by the focusing lattice in tank 1. Including the flutter factor, however, the beams grow to about the same size at the end of the linac in both examples as we see in figures 36 and 37.

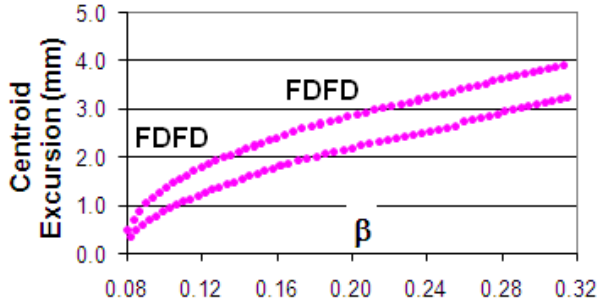

Figure 34. Reference FDFD Expected Centroid Excursion with Errors

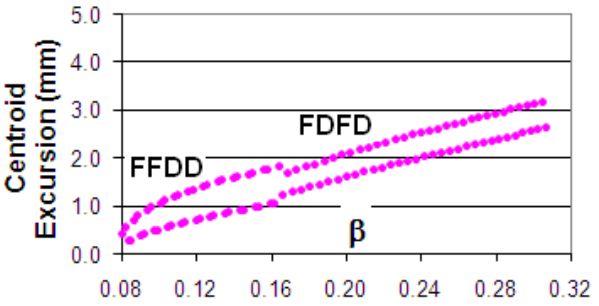

Figure 35. Reference FFDD Expected Centroid Excursion with Errors

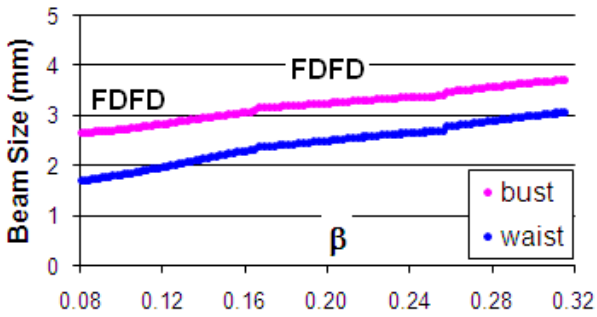

Figure 36. Reference FDFD Equivalent Uniform Beam Size

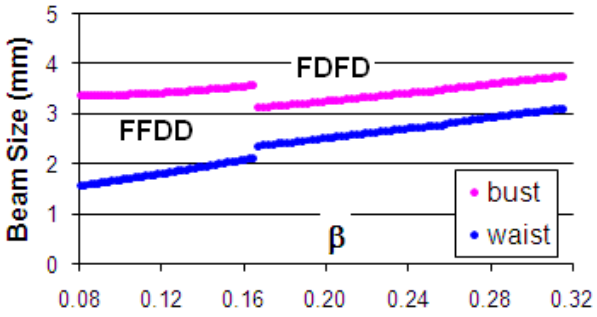

Figure 37. Reference FFDD Equivalent Uniform Beam Size

Adding the beam bust size to the expected centroid excursion and converting to a 3σ Gaussian beam, figures 38 and 39 show that the FFDD lattice in tank 1 provides slightly better expected performance.

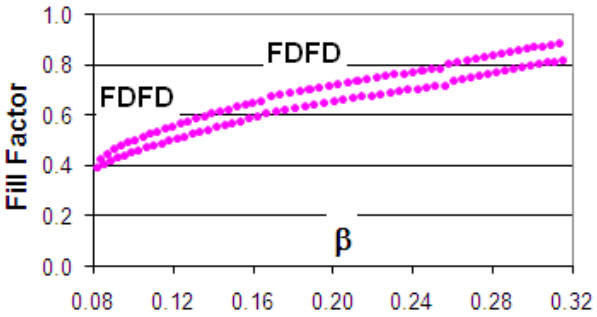

Figure 38. Reference FDFD Expected Filling Factor for a 3σ Beam

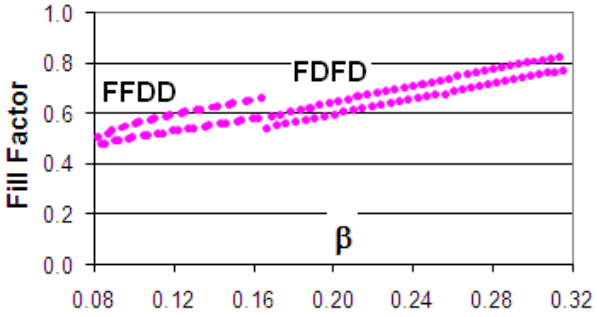

Figure 39. Reference FFDD Expected Beam Filling Factor for a 3σ Beam

8. Baseline and Reference Designs with an FFDD Lattice Throughout.

The logic for considering an FFDD lattice in tank 1 was to facilitate the transverse match from the chopper line. In addition the quadrupole gradient required in the initial quadrupole is 100 T/m in the FDFD design while it is about half that value in the FFDD case. The same argument would support a longer lattice period at the end of the DTL to facilitate the DTL to CCDTL match. The FFDD lattice has the added advantage of requiring weaker PMQs in all drift tubes.

The logic for starting with and maintaining a larger synchronous phase, φ_s, creating a larger longitudinal acceptance in the Reference design was to capture more of the debunched beam from the chopper line and make the linac performance less sensitive to rf phase and amplitude errors. We can see the effect of this in figures 40 and 41 which show the width in real space of the separatrix in the two designs. The Reference design intentionally maintains a larger separatrix over a longer distance as the cell lengths grow longer. In effect this adiabatically shrinks the "bucket" relative to $\beta\lambda$ in tank 1. The discontinuity at the end of tank 1 in figure 41 reflects the discontinuities in φ_s and E_0 shown in figure 4. In this design E_0 was reduced in an attempt to conserve power. φ_s was then tailored to keep the longitudinal real estate phase advance smooth as shown in figure 12.

A consequence of this design is that it drives up the length, the number of drift tubes and the power requirements in tanks 1 and 2 so a compromise is probably indicated. To support this decision we have finally considered the option of extending the FFDD lattice throughout the linac in both the Baseline and Reference designs.

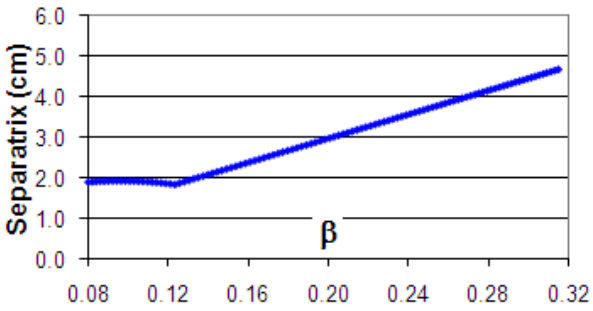

Figure 40. Baseline Design Separatrix Phase Width

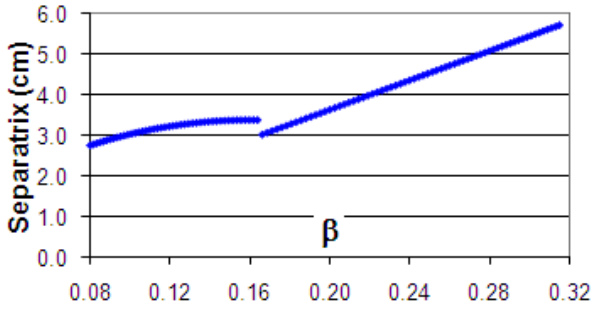

Figure 41. Reference Design Separatrix Phase Width

As expected, figures 42 and 43 show a slightly depressed equipartitioning ratio, in both the Baseline and the Reference linacs, having FFDD focusing lattice throughout. This tells us that, with a well-matched initial beam, we should expect minimal emittance growth due to energy exchange between planes in both designs even if the longitudinal emittance is larger than expected. The Hofmann Diagrams in figures 44 and 45 show that the coupled motion safely lies between the resonance bands in both designs. As in figures 31 and 33 we can again see the consequences of having to tailor the quadrupole strengths to avoid the σ_{0t}=90°.

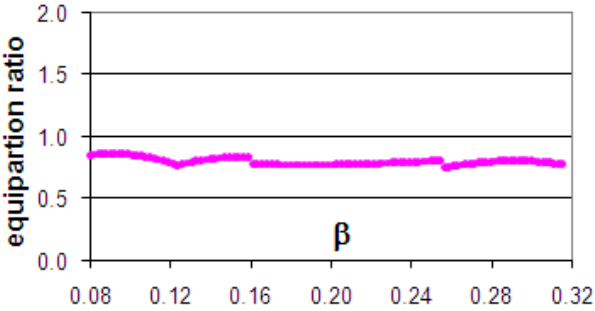

Figure 42. Baseline FFDD Throughout Equipartitioning Ratio

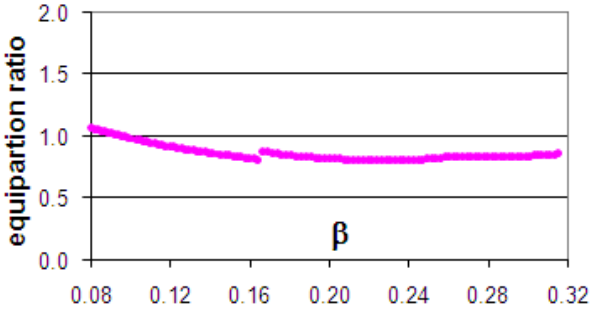

Figure 43. Reference FFDD Throughout Equipartitioning Ratio

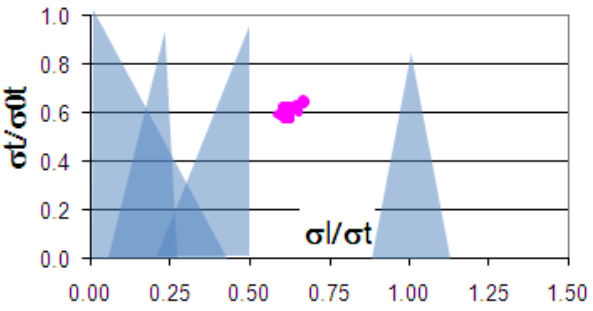

Figure 44. Baseline FFDD Throughout Hofmann Diagram

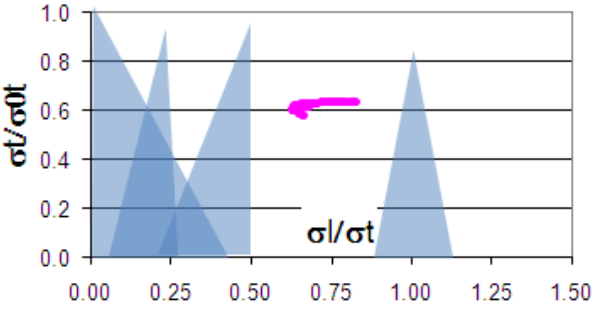

Figure 45. Reference FFDD Throughout Hofmann Diagram

We see in figures 46 and 47 that the expected centroid excursion is just slightly larger in the Reference design that has 4 more cells. The quadrupole strengths are slightly stronger in the Reference design as well which keeps the matched beam slightly smaller as shown in figures 48 and 49. As a result there is essentially no difference in the expected filling factors as shown in figures 50 and 51.

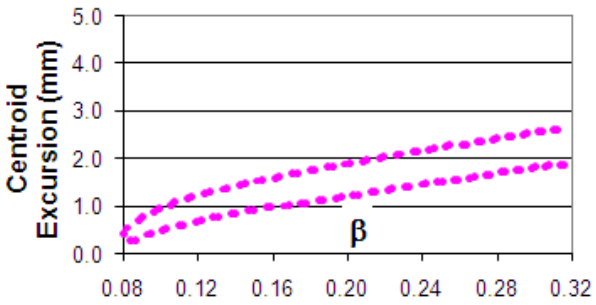

Figure 46. Baseline FFDD Throughout Centroid Excursion

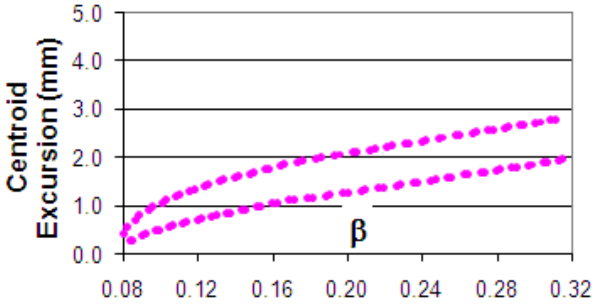

Figure 47. Reference FFDD Throughout Centroid Excursion

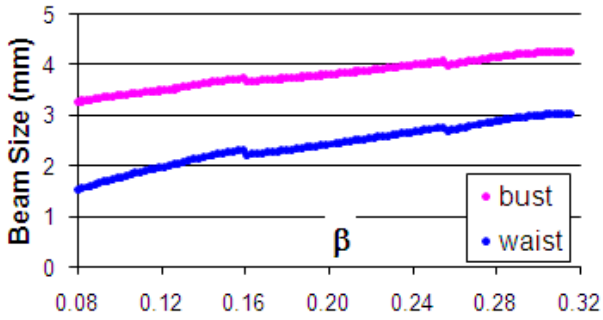

Figure 48. Baseline FFDD Throughout Waist & Bust

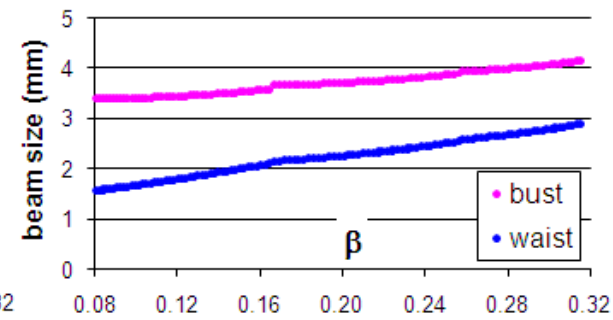

Figure 49. Reference FFDD Throughout Waist & Bust

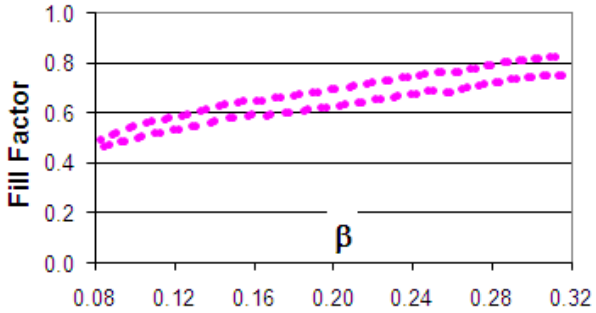

Figure 50. Baseline FFDD Throughout Filling Factor for a 3σ Gaussian Beam

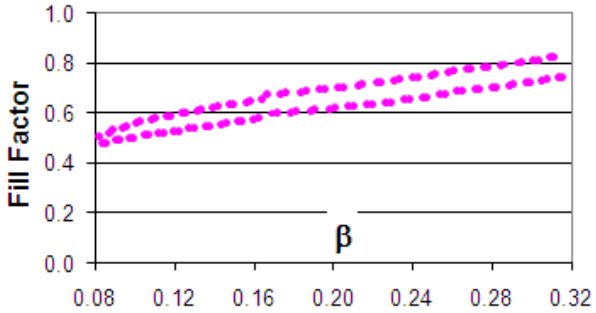

Figure 51. Reference FFDD Expected Filling Factor for a 3σ Gaussian Beam

Looking statistically at the centroid excursion with errors, LTRACE shows in figure 52 the Baseline design to be slightly better as predicted by DTLTOOL. Figure 53, however shows no difference in the filling factor. There is about a 12% chance in the either design that we would be so unfortunate to have misalignments that resulted in a 3σ beam touching the bore. Figure 54 shows where the largest filling factors occur in the 1000 cases corresponding to the probability chart.

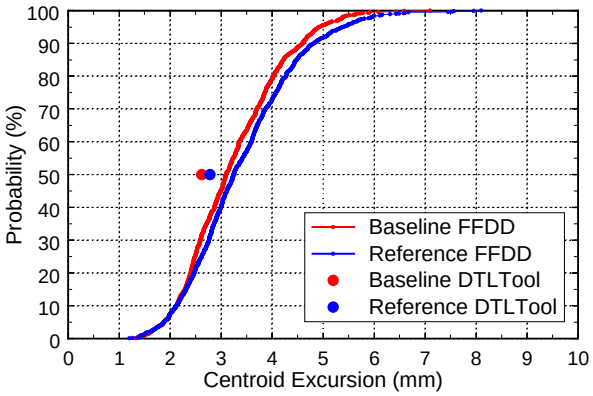

Figure 52. Centroid Excursion Probability for Baseline and Reference Designs with FFDD Throughout

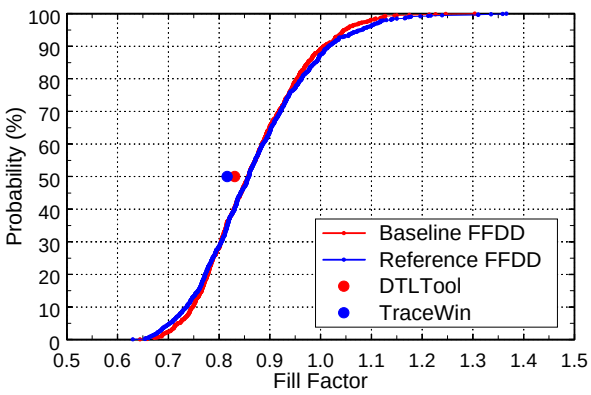

Figure 53. Filling Factor Probability for for Baseline and Reference Designs with FFDD Throughout

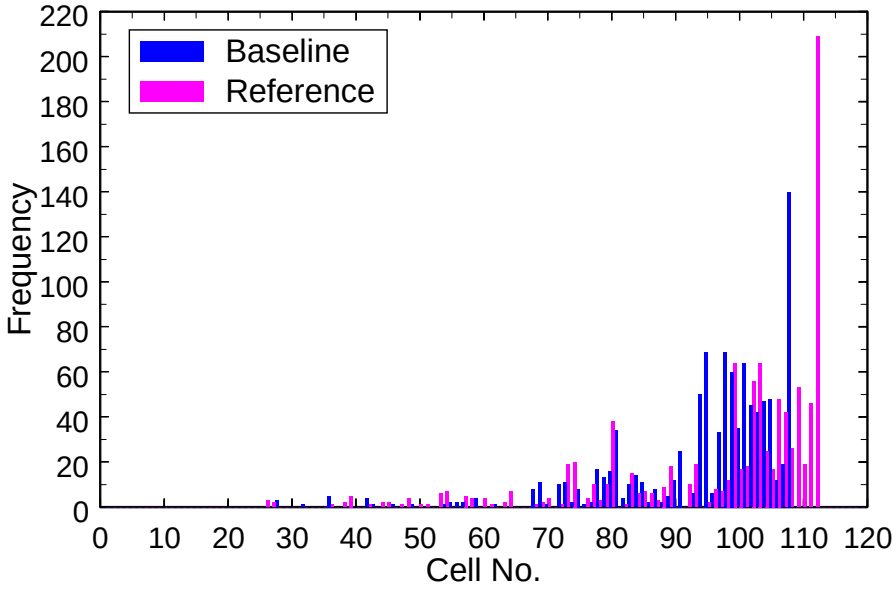

Figure 54. Expected distribution of Maximum Filling Factor for Baseline and Reference Designs with FFDD throughout for 1000 error sets in each case

Examining the beam properties in the defocusing quadrupole at the end of each linac from TRACEWIN simulations, figures 55 and 56 show the transverse profiles to be very similar, with the Reference design being slightly narrower and having a smaller halo. Adding the 3σ size from the Baseline design simulation to the expected centroid excursion gives us an expected filling factor of 84% compared to 83% calculated by DTLTOOL. Adding the 3σ size from the Reference design simulation to the expected centroid excursion gives us an expected filling factor of 82% compared to 83% calculated by DTLTOOL. Although it is not obvious, the halos extend to almost 9 mm in both cases so even in the most optimistic case of misalignments some beam would be lost.

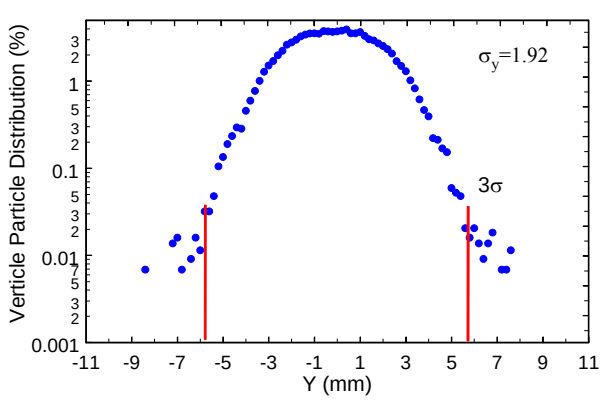

Figure 55. Log Plot of Vertical Profile in Final Quad of Baseline with FFDD Throughout

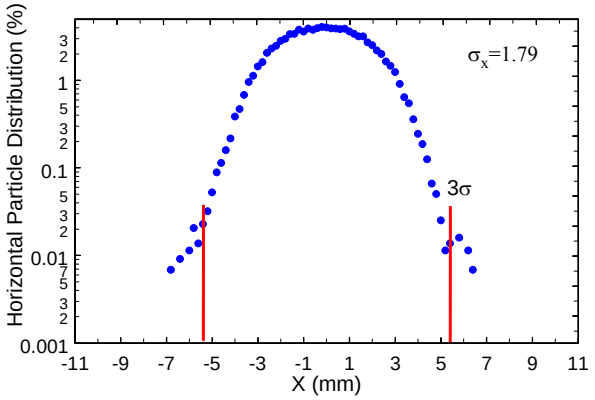

Figure 56. Log Plot of Horizontal Profile in Final Quad of Reference with FFDD Throughout

Since the motivation for the Reference design was to improve the beam performance in the presence of phase and amplitude errors we looked briefly at the longitudinal emittance to make sure that there is no unexpected degradation resulting from the FFDD lattice. Figures 57 and 58 show the longitudinal phase-space projections of the beam at the exit of the Reference linac with FDFD and FFDD focusing lattices simulated by PATH (1). There is no significant difference. If we estimate the phase width for ~99% of the beam to lie within ~20°, then we can see that it would occupy ~25% of the longitudinal acceptance at the linac exit as shown in figure 41.

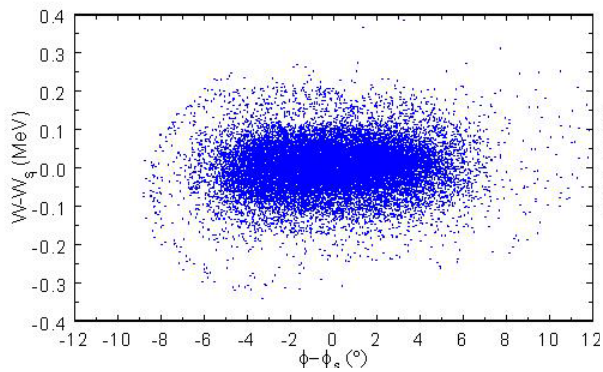

Figure 57. Longitudinal Phase-Space at Exit of Reference FDFD with Throughout

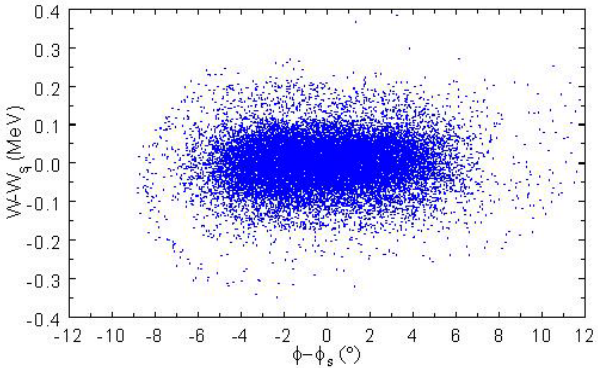

Figure 58. Longitudinal Phase-Space at exit of Reference with FFDD Throughout

9. Conclusions.

Based on these analyses and our present understanding of beam dynamics in linacs, we can conclude that both the Baseline and Reference linac designs are generally conservative with respect to the selection of transverse and longitudinal restoring forces, stable motion and the avoidance of potential resonances.

We observe minor differences in the transverse performance of both designs with different transverse focusing lattices. In none of the cases studied can we realistically expect to accelerate beam without loss in the absence of steering. Based on the consistent results from three approaches we recommend adopting an FFDD lattice throughout as 1) having the lower expected beam loss in the presence of alignment errors and 2) requiring lower magnetic field gradients.

We propose to carry out similar studies on a "final" design to confirm this recommendation. Initial studies indicate that if we can find appropriate locations for steering elements, we might improve the transverse performance. We therefore propose to further examine our options for fine tuning the FFDD lattice to facilitate steering in the final design.

10. Bibliography

1. *CEA Saclay Codes Review.* **Duperrier, R., Pichoff, N., Uriot, D.** Amsterdam, 2002. ICCS Conference.
2. **Stovall, J.** private communication.
3. **Billen, J. H. and Young, L.M.** *Poisson Superfish,* Los Alamos National Laboratory. LA-UR-96-1834 (revision January 13, 2006).
4. **Rusthoi, K.R. Crandall and D.P.** *TRACE3-D Documentation,* Los Alamos National Laboratory. LA-UR-97-886 (third edition, May 1997).
5. *Emittance Coupling in High Intensity Beams Applied to the SNS Linac.* **Hofmann, I., Franchetti, G., Boine-Frankenheim, O., Qiang, J., Ryne, R., Jeon, D., Wei, J.** Chicago : Particle Accelerator Conference, 2001.
6. **Galambos, J.** private communication.
7. **Crandall, K.R.** private communication.
8. **Perrin, A., Amand, A.F.** *Travel v4.06, User Manual,* CERN, 2003.